JPE Journal of Photonics for Energy

RESEARCH PAPER

Impact of grass retroreflection on bifacial solar panel electricity yield in agrivoltaics

Jelle Westerhof,[a] Leonie M. Horst,[a] Anne Rikhof,[a] Shweta S. Pal,[a] Dmitry Busko,[b] Bryce S. Richards,[b,c] and Rebecca Saive[a,*]

[a]University of Twente, MESA+ Institute for Nanotechnology, Inorganic Materials Science, Enschede, The Netherlands

[b]Karlsruhe Institute of Technology, Institute of Microstructure Technology, Eggenstein-Leopoldshafen, Germany

[c]Karlsruhe Institute of Technology, Light Technology Institute, Karlsruhe, Germany

ABSTRACT. The efficiency of bifacial photovoltaic modules, which can capture light from both sides, is significantly influenced by the reflectivity of the surrounding environment, for example in agrivoltaic settings. We investigate the retroreflective properties of grass and their impact on the energy yield of bifacial solar panels. By combining spectro-angular reflection measurements with computational modeling, we quantify the contribution of grass reflection to overall solar electricity production and evaluate the inaccuracies associated with the assumption that grass behaves as a diffuse reflector. Our results show that this assumption can lead to an overestimation of energy yield by up to 10%, due to the actual retroreflective behavior of grass. This effect is particularly pronounced for long grass configurations. The research underscores the importance of considering the detailed reflectance properties of vegetation in optimizing the placement and performance of bifacial photovoltaics in agricultural environments, with implications for improving the efficiency and sustainability of solar energy generation.

Keywords: agrivoltaics; spectro-angular albedo; photovoltaic yield simulation; grass; canopy hotspot

Paper 24048SS received Sep. 26, 2024; revised Dec. 17, 2024; accepted Dec. 24, 2024; published Jan. 16, 2025.

1 Introduction

The advancement of solar energy technology has led to innovations designed to maximize energy capture efficiency. Among these, bifacial photovoltaic (PV) modules have emerged as a promising solution to increase electricity production.[1,2] Bifacial solar panels can capture direct and diffuse sunlight from both the front and rear sides, efficiently utilizing light reflected from surrounding surfaces and the environment, thereby potentially increasing their overall power output.[3] Furthermore, bifacial modules present new opportunities for integration in settings such as agriculture ("agrivoltaics")[4–7] and building-integrated photovoltaics.[8–11]

However, the efficiency of bifacial solar panels is intricately tied to various environmental factors, including the reflectivity of the surroundings, i.e., the albedo.[8,12] Reflectors are often evaluated using the averaged albedo, both spectrally and angularly.[8,13] The spectral dependence of the albedo and its influence on the yield of photovoltaic devices have been widely studied[14–17] and must be considered for an accurate electricity yield prediction.[11]

*Address all correspondence to Rebecca Saive, r.saive@utwente.nl

In recent work,[18,19] we have shown the influence of the angular albedo properties on PV electricity generation. Spectro-angular albedo is material-dependent and can be broken down into three components, a glossy component, a specular or mirror-like component, and a diffuse component. A diffuse reflector scatters the light in all directions following a Lambertian distribution, a specular reflector reflects the light such as a mirror, and a glossy reflector reflects the light with a lobe around the mirror angle.[18] The glossy component can be modeled using the GGX theory.[20] Together, these three components determine the angular dependence of the reflectivity. The model introduced in the above-cited work can provide accurate predictions of PV energy yield as demonstrated by comparison with experiments.[18]

However, the aforementioned model assumes macroscopically flat surfaces, such as paint or concrete. In the case of agrivoltaics, this assumption is not valid, as the panels are surrounded by crops and plants such as grass. Although individual leaves, as we will confirm in this study, are diffuse, and can thus be described by the model, the overall macroscopic structure results in different reflection properties. In addition, the reflectance is known to depend on the leaf geometry and water content.[21–23] The reflectance of grass and trees has been studied in various fields such as computer graphics[24] and Earth observation.[25,26] Canopies, the upper layer of vegetation formed by the crowns of trees or plants that provide cover and shade, are known to exhibit retroreflective behavior.[27] A retroreflective surface reflects light back toward its source with minimal scattering, regardless of the angle of incidence. Due to the slight tilt of grass leaves, grass can be considered to form a canopy. In the case of canopies, the emergence of this regime of high reflectivity close to the angle of incidence is referred to as the hot spot.[27,28] As incident light hits the foliage (i.e., the collective leaves of a plant or tree) the light is scattered in different directions. Subsequently, this scattered light can hit different leaves, before exiting the canopy or being absorbed. The predominant route for light to exit the canopy while minimizing absorption is to retrace its initial path of entry, resulting in retroreflection, and therefore enhanced backscattered light intensity.

In this paper, we explore the influence of the retroreflective properties of grass on the electricity yield of bifacial solar panels. Using spectro-angular reflection measurements and computational modeling, we quantify the contribution of grass retroreflection to bifacial solar panel energy production and assess the errors from assuming grass behaves as a diffuse reflector. In addition, by changing the morphology of the different simulated grass samples, we study the influence of the grass geometry on the reflection properties. This research seeks to inform strategies to optimize the placement and design of solar panels in grass-rich environments, such as agrivoltaics, ultimately advancing the efficiency and sustainability of solar energy generation in an agrivoltaic setting.

2 Materials and Methods

2.1 Spectro-Angular Reflection Measurements

To perform spectro-angular reflection measurements, we used a spectrophotometer (Agilent Cary 7000) equipped with a universal measurement accessory (UMA). This spectrophotometer has a tunable monochromatic light source. By sweeping over a spectral range from 400 to 1000 nm, we obtained the reflection spectra. A goniometer was used to measure reflection at various elevation angles of incidence from 30 deg to 90 deg, with 20 deg increments. The detector's position was moved from 5 deg to 90 deg in 5 deg increments. Both the sample and the detector were rotated; the sample was to vary the angle of incidence α_i and the detector was to record the reflectivity at corresponding angles α_r. Figure 1(a) contains a schematic of this setup. The shape of the spectrum remains consistent across different angles of reflection, with only the magnitude varying. Consequently, we measured the full spectrum for a limited number of angles, whereas for all other angles, we took measurements at 550 nm, in which grass has a reflection peak.

Our samples consisted of a mixture of several grass subspecies. This mixture is typically used in lawns. The grass samples contained ~20% English ryegrass (*Lolium perenne*), split evenly between diploid and tetraploid subspecies, and 30% smooth meadow grass (*Poa pratensis*). The remaining 50% consists of several subspecies of the red fescue (*Festuca rubra*): 20% of *trichophylla*, 20% of *commutata*, and 10% of *rubra*. The longest grass blades measured ~10 to 12 cm, and the grass was regularly watered to prevent drying. We also measured

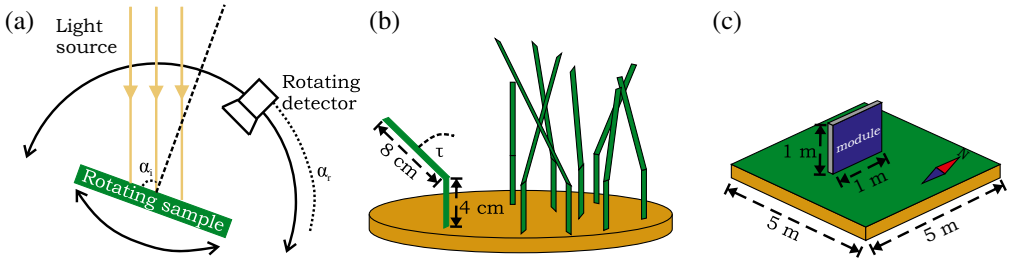

Fig. 1 (a) Schematic of the goniometer setup used to perform the spectro-angular reflection measurements. The source, rotating sample stage, and rotating detector are indicated. (b) Schematic of a grass sample as created for the Monte Carlo ray tracing model. Each blade is modeled as a flat vertical surface with a width of 0.5 cm, a non-tilted bottom of 4 cm, and a 40-deg zenithally tilted top of 8 cm. The blades are randomly azimuthally rotated. (c) Schematic of the configuration used as input for the ray tracing software of[18] to calculate the yield of the east-west facing vertical bifacial module. The 1×1 m^2 module is placed 0.25 m above the 5×5 m^2 reflector.

individual grass leaves to confirm that the retroreflectivity of the grass is a cumulative result of the canopy.

2.2 Monte Carlo Ray-Tracing Simulations

In addition to the measurements, we performed simulations using an in-house Monte Carlo ray-tracing model. More information on the model and its validation can be found in the master thesis by Horst.[29] Using this model, we computed the tabulated biderectional reflection distribution function (BRDF)[30] of different grass samples. Each grass sample consists of a flat, vertically positioned surface, with an additional flat surface placed on top at a random tilt. The height and tilt of these surfaces vary between samples. For the reflection of each surface, spectral data are taken from Russel et al.[15] for grass and from Baldridge et al.[31] for the soil. All individual surfaces are modeled as diffuse reflectors. We consider two different samples, one in which the grass is long and one in which the grass is short. The size of the simulated long grass is comparable to the size of the measured grass. For long grass, leaves have a base of 4 cm and a top of 8 cm, with a maximum random tilt of 40 deg. For short grass, leaves have a base of 2 cm and a top of 2 cm, with a maximum tilt of 20 deg. For both samples, the soil is represented by a flat round surface with a radius of 5 cm, and each sample consists of 180 grass blades. This corresponds to a blade density of 22,900 per square meter. Grass blade density is known to vary significantly,[32,33] making a soil sample potentially unrepresentative. To address this, we adopted a commonly used value for artificial grass.[34] Figure 1(b) provides a schematic of the long grass sample.

To compute the BRDF, we generate a bundle of 100,000 parallel rays, all uniformly distributed across the grass surface. When a ray strikes a surface, it changes both direction and intensity, following the Lambertian distribution of a diffuse reflector, with its spectral magnitude adjusted based on the reflectance of grass and soil. We assume no transmission, so all light is either reflected or absorbed. Rays are considered fully absorbed if their magnitude drops below 1% of the original. A detection dome, divided into 6 deg by 6 deg pixels for both azimuth and elevation angles, registers the magnitude of each ray leaving the system. After each ray has either been detected or fully absorbed, the BRDF is calculated for that angle of incidence.

We calculate the BRDF for ten samples with random orientations and average the results to minimize the effects of randomness. This process is repeated for different elevation angles of incidence, from 0 deg to 66 deg in 6 deg increments. These angles capture the Sun's elevation angles during summer in Germany. The azimuth angle remains constant, as the random orientation of samples eliminates its effect on the BRDF.

2.3 Photovoltaic Yield Simulations

The computed BRDF for each angle of incidence is then implemented in the ray tracing model presented by Pal et al.[18] and Rikhof et al.[35] to calculate the yield of photovoltaic devices. For this, as shown in Fig. 1(c), a 1×1 m^2 east-west facing bifacial PV module is placed 25 cm above a 5×5 m^2 reflector. The module is assumed to have a fill factor of 0.85 and an open circuit voltage

of 730 mV. Under standard AM1.5G conditions, the simulated panel has a short-circuit current density of 34.37 $\mathrm{mA/cm^2}$, calculated by integrating over the external quantum efficiency (EQE). This results in 213 Wp for a 1 $\mathrm{m^2}$ panel. The panel has a bifaciality of 98.8%. These parameters match those used by Russel et al.[15] We assume that the open circuit voltage and the fill factor remain constant, and we do not consider temperature changes in the module. We consider four distinct configurations for the reflector beneath the panel: two with the BRDF of grass, as computed by the Monte Carlo ray-tracing model for long and short grass, respectively; one where we take grass to be a diffuse reflector; and one without any reflector present. Irradiance data can then be used to calculate the normalized specific yield of this configuration. As irradiance data, we use data measured at an agricultural solar farm in Aasen, Germany (47 59′ 00″ N, 8 33′ 00″ E), from Next2Sun Technology GmbH. The grass at this farm was mowed on July 5, 2022. To compare the yield before and after mowing, we consider the irradiance data from July 2 and July 8, as these days were similar in solar irradiance and temperature.

3 Results

3.1 Results of the Reflection Measurements and Ray-Tracing Simulations

Figure 2(a) contains a picture of a grass sample inside the spectrophotometer. In Fig. 2(b), we show the spectrum of the grass sample for an angle of incidence of $\alpha_i = 70$ deg and a reflection angle of $\alpha_r = 50$ deg. The spectrum exhibits the characteristic features of grass, including a prominent peak at 550 nm and high reflection in the infrared region between 700 and 1000 nm. In Fig. 2(c), the angle-dependent reflection properties of a single grass blade are shown. The Lambertian behavior of the reflectance, as fitted, confirms that single grass leaves scatter the light diffusely. By contrast, Figs. 2(d)–2(f) shows that for a full grass sample at various angles of incidence, the canopy's obscuring structure causes the most scattered light to be reflected back toward the source. This is also evident in the lower magnitude in the BRDF when comparing the full samples, as shown in Figs. 2(d)–2(f), to the single leaves as shown in Fig. 2(c). In these graphs, blue and green dots represent a cross-section of the three-dimensional BRDF, computed using the Monte Carlo ray-tracing model. The simulations show similar retroreflective effects to

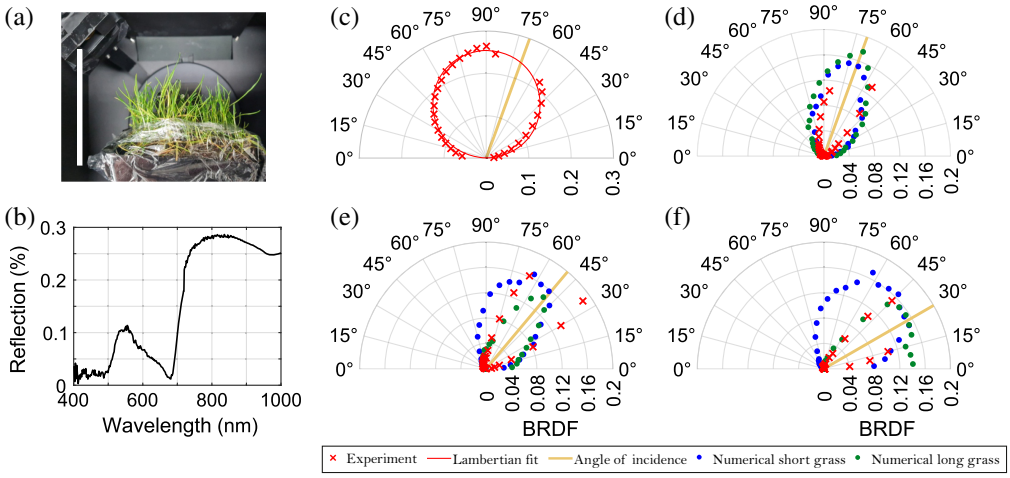

Fig. 2 (a) Picture of the grass inside of the goniometer setup. The grass is on a stage that can rotate to change the angle of incidence. The detector is shown in the top left of the picture. The white scale bar represents ~15 cm. (b) Measured spectral reflectance of the grass sample at an elevation angle of incidence of $\alpha_i = 70$ deg and a reflection angle of $\alpha_r = 50$ deg. (c) Measured angular reflection of single flat grass leaves. The red solid line is a Lambertian fit. (d)–(f) Measured and computed angular reflection of grass for an angle of incidence of (d) 70 deg, (e) 50 deg, and (f) 30 deg. In each case, for the numerically calculated reflection, the short grass has a bottom of 2 cm, a top of 2 cm, and a maximum tilt of 20 deg and the long grass has a bottom of 4 cm and a top of 8 cm and a maximum tilt of 40 deg. The BRDF of the simulations has been multiplied by a factor of 5 to match the numerical aperture of the experiments.

those observed in the experiments. The differences between experiments and simulations can be attributed to the fact that the morphology of the simulations and the measured grass are not the same. In the simulations, because all surfaces are flat, more light is reflected at grazing angles. This effect is particularly pronounced in the long grass simulation at a 30-deg incidence angle, as shown in Fig. 2(f). Close to a normal incidence, as shown in Fig. 2(d), there is a good match between the experiments and the simulations, and the structure of the grass has less influence on reflection. For the simulation, the reflection curves are not completely continuous; this is caused by deviations in the sample structures. Although averaging reduces these variations, some discrepancies in the reflection curves remain.

The BRDF is shown for both short and long grass in Fig. 3. Figures 3(a) and 3(e) show the model-generated samples, whereas Figs. 3(b)–3(d) and 3(f)–3(h) illustrate the tabulated BRDF for increasing angles of incidence for short and long grass, respectively. The angle of incidence is indicated by the yellow line in the figure. For both types of grass, the reflection forms a lobe around the angle of incidence, thus indicating a hot spot. Because the leaves in long grass are longer and more tilted, the canopy effect is more pronounced, leading to greater retroreflection than in short grass. This is especially apparent for the closer-to-grazing angles of incidence, where the short grass reflects more light upward compared with the long grass. Closer to normal incidence, the reflection intensity for both types of grass is comparable. In this case, as the grass is largely vertical, many of the rays hit the soil, which diffusely scatters light equally for both long and short grass.

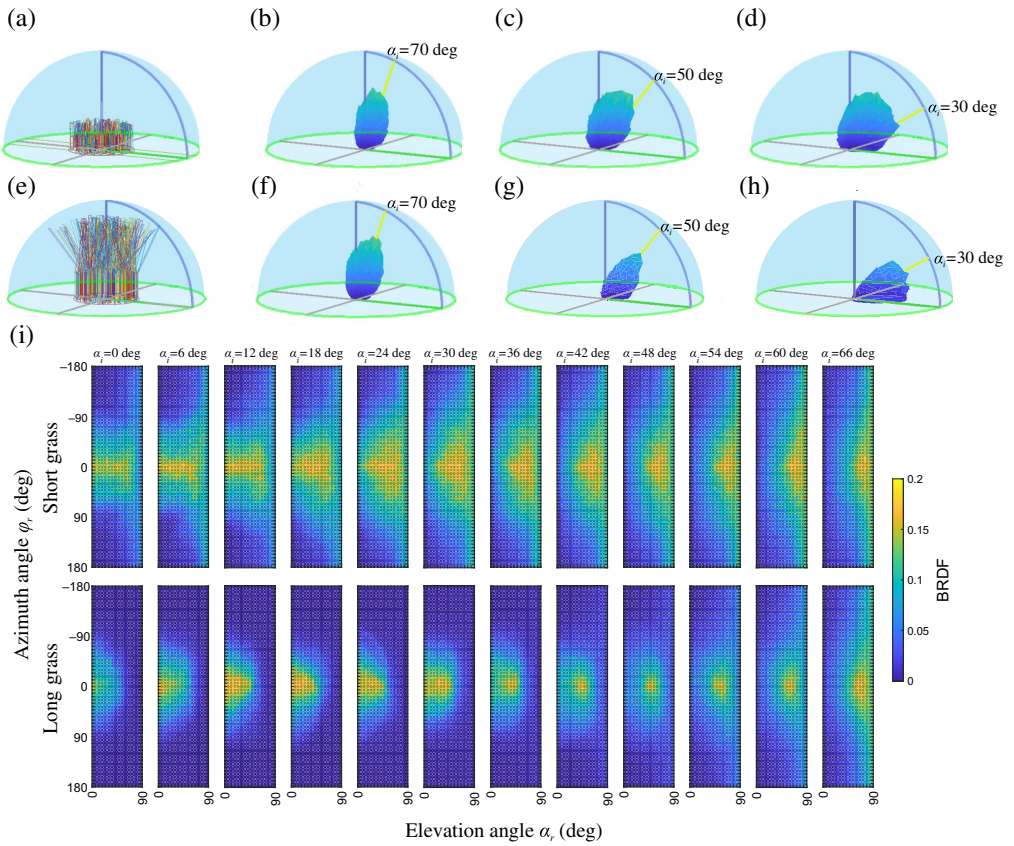

Fig. 3 (a) Example of short grass as created by the model with a bottom of 2 cm, a tilted top of 2 cm, and a maximum tilt of 20 deg. (b)–(d) Simulated 3D BRDF average of 10 samples with short grass for various angles of incidence. (e) Example of long grass as created by the model with a bottom of 4 cm, a tilted top of 8 cm, and a maximum tilt of 40 deg. (f)–(h) Simulated 3D BRDF average of 10 samples with long grass for various angles of incidence. (i) Heatmaps of the simulated BRDF of the short (top row) and long grass (bottom row) for angles of incidence between 0 deg and 66 deg with a step size of 6 deg.

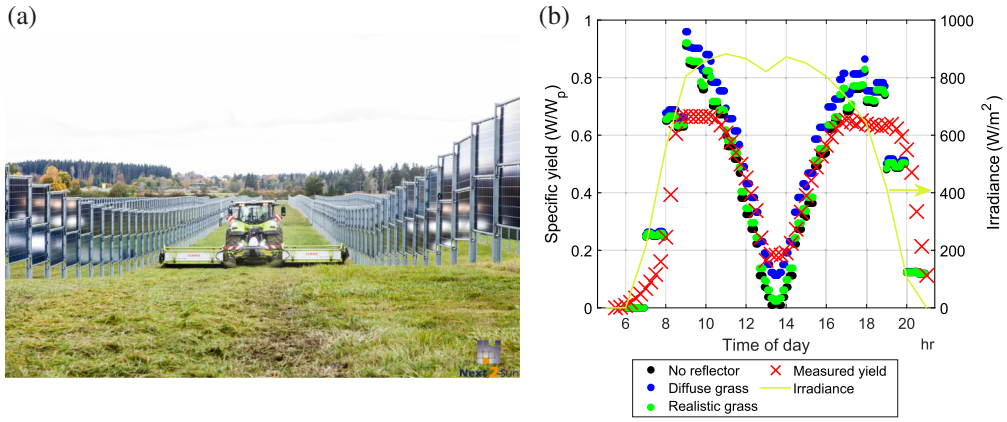

Fig. 4 (a) A picture of the agricultural solar farm in Aasen. (b) The simulated yield of a 1×1 m^2 PV panel on top of a 5×5 m reflector with the BRDF of the long grass (green) and when the grass is assumed to be diffuse (blue). The simulation for the case without a reflector is also shown in black. The irradiance data, as shown in yellow and belonging to the right *y*-axis, used to perform these simulations were obtained on July 2, 2022, by Next2Sun GmbH. In red, the measured specific yield of Next2Sun's agricultural solar plant in Aasen 3 days before the mowing of the grass. The power generation is capped at 62% of the watt peak by the inverter to avoid net congestion.

3.2 Results of the Yield Simulations

To estimate bifacial solar panel yield in an agricultural environment and quantify the impact of mowing, we simulated the yield of a vertical east-west facing panel placed above a horizontal reflector. For the reflection surface, we used the computed BRDF of the long and short grass. Figure 3(i) shows the full BRDF for all angles of incidence relevant to the elevation of the Sun in Germany. For comparison, we also show the simulated yield of a module without a reflector. To quantify the error from assuming that grass reflects diffusely, we also simulate a configuration with a diffuse reflector using the spectral reflection of grass. We compare the results from the simulations to power generation data from a 4.1 MWp agricultural solar farm from Next2Sun Technology GmbH. Figure 4(a) contains a picture of this solar farm which is located in Aasen, Germany. The irradiance data used for the simulations were collected at this solar farm and are shown in Fig. 4(b). The data were collected on a vertically oriented surface at hourly intervals.

The grass at this agricultural solar farm was mowed on July 5, 2022. In the days following mowing, the plant's yield increased by up to 6.6%. This increase can only partly be attributed to an increase in irradiance. Figure 4(b) shows the measured yield of the solar farm on July 2, before mowing. The east-west orientation of the modules results in two distinct peaks in energy yield: one in the morning and another in the afternoon. There is a noticeable drop near noon when the Sun is at its highest point in the southern sky, illuminating the edge of the bifacial PV module. Figure 4(b) also shows the simulated yields for various reflector types. As expected, direct sunlight, represented by the configuration without a reflector, contributes the majority of the total yield. However, when assuming diffuse grass reflection, the yield over the day is overestimated by 10.5% compared with the simulation with the BRDF of long grass. This overestimation is particularly noticeable around midday when the incoming sunlight is parallel to the module. At its peak, the PV panel generates 0.91 W per W_p under direct sunlight. When a configuration with a reflector is considered, assuming diffuse reflection from grass, the peak output increases to 0.96 W per W_p. When we instead consider the more realistic BRDF for long grass, the peak output of the panel reaches 0.92 W per W_p. The minimum output, occurring at solar noon, is 0 W per W_p, 0.11 W per W_p, and 0.02 W per W_p for the three configurations, respectively. For the measured yield, at its peak, the plant produces 0.62 W per W_p, which is lower than the simulated values due to power generation limitations. These can be attributed to the inverter or the grid to avoid congestion issues. During solar noon, the plant produced 0.16 W per W_p. These results are summarized in Table 1. The average difference in the yield throughout the day between the configuration where we consider diffuse grass and realistic grass is 0.041 W per W_p.

Table 1 Minimum and maximum value of the yield as a ratio of the W_p value for the measured yield and the different simulated configurations. For the measured yield, the maximum yield value is low due to power generation limitations.

Configuration	Minimum yield (W/W_p)	Maximum yield (W/W_p)
Measured yield	0.16	0.62
No reflector	0	0.91
Diffuse grass	0.11	0.96
Realistic long grass	0.02	0.92

The simulation exhibits significant fluctuations in power generation, especially during the morning and afternoon hours. These fluctuations result from the use of hourly irradiance data, whereas the simulation operates at 5-min intervals, continuously updating the Sun's position. Around the solar noon, when irradiance remains relatively stable, these fluctuations are minimized.

The decrease in power generation at solar noon is more pronounced in the simulation compared to the measurements. This discrepancy is likely due to the higher amount of diffuse light scattered by the sky and surroundings in the measured scenario, which the simulation cannot fully capture. The simulation assumed only direct irradiance and did not include diffuse irradiance. In addition, the simulation setup is limited to a 5×5 m^2 reflector, with no other elements or structures surrounding the panel that might contribute to the scattering of light. By contrast, real-world measurements are influenced by a more complex environment where diffuse light from various sources enhances the total irradiance on the panel. The restrictions on maximum power generation imposed by the inverter and the grid make the comparison between simulation and measurements more challenging. Unfortunately, no days near the mowing date had comparable irradiance conditions without power generation limits. This lack of unrestricted data complicates the validation of the simulation model, making it harder to draw direct comparisons or conclusions. Despite this, the simulation using the same irradiance data and BRDF for short and long grass shows that the short grass configuration yields 1% more than the long grass. As illustrated in Fig. 3, long grass reflects a higher ratio of light back toward the source. Consequently, less light reaches the solar panel, resulting in a slightly reduced yield compared to short grass and only marginally higher than the no-reflector scenario. When using the BRDF of short grass for the reflector and irradiance data on July 8, 2022, post-mowing, the increase in the simulated electricity yield is 6.9%, closely matching the measured increase of 6.6%. This suggests that maintaining short grass and mowing regularly could increase the yield of the plant. It should be noted that mowed grass also reflects a somewhat different spectrum as is typically evident by the more yellow color. This effect was not taken into account in this study and would require accurate spectral albedo measurements before and after mowing. The effect of fluctuations in the spectral albedo has been studied by Barragán Sánchez-Lanuza et al.[36]

4 Conclusion

We have studied both experimentally and computationally the hotspot retroreflective effect of grass caused by its canopy. Using the computed three-dimensional BRDF, we calculated the yield of a bifacial solar panel under near-realistic conditions. Our results show that assuming diffuse grass leads to an overestimation of the yield by up to 10.5%. Simulation data indicate that long grass contributes only marginally to solar panel yield, favoring short grass for higher yield. Future research could be devoted to the investigation of the impact of various types of crops on photovoltaic yield considering their full spectro-angular reflectance properties. In addition, it would be instructive to study how additional environmental factors, such as water content and weather effects such as wind, influence grass and other crop reflectance. Our findings highlight the importance of considering these nuanced factors when forecasting solar panel output in agricultural environments. Furthermore, our study contributes to the broader discourse on the integration of renewable energy in agricultural systems, highlighting the need for customized approaches to maximize efficiency and sustainability.

Disclosures

The authors declare no competing financial interest.

Code and Data Availability

The data that underlie the plots in this paper, the Monte Carlo ray tracing code, and other findings of this study are publicly available on data.4tu.nl and from the corresponding author on reasonable request.

Acknowledgments

The authors would like to thank Peter Bendix, Simon Lahr, and Anna Morales Vilches from Next2Sun Technology GmbH for providing the irradiance, temperature, and yield data of their vertical solar power plant in Aasen, Germany, and for helpful discussions and insights. During the preparation of this work, J. Westerhof used ChatGPT and Writefull to edit some sections of the text to improve readability. After using this tool/service, J. Westerhof reviewed and edited the content as needed and took full responsibility for the content of the publication. This publication is part of the project Diffuse Irradiance Redirector for Efficient ConcenTration (DIRECT) with project number KICH1.ED02.20.006 of the research program NWO Kennis- en innovatieconvenant Innovations for Wind and Solar which is (partly) financed by the Dutch Research Council (NWO). The KIT team was supported by the Helmholtz Association – Research Field Energy – Materials and Technologies for the Energy Transition program (Topic 1 Photovoltaics and Wind Energy, 38.01.05).

References

1. R. Guerrero-Lemus et al., "Bifacial solar photovoltaics–a technology review," *Renew. Sustain. Energy Rev.* **60**, 1533–1549 (2016).
2. J. Zhong et al., "Development and challenges of bifacial photovoltaic technology and application in buildings: a review," *Renew. Sustain. Energy Rev.* **187**, 113706 (2023).
3. A. Cuevas et al., "50 Per cent more output power from an albedo-collecting flat panel using bifacial solar cells," *Sol. Energy* **29**, 419–420 (1982).
4. H. Dinesh and J. M. Pearce, "The potential of agrivoltaic systems," *Renew. Sustain. Energy Rev.* **54**, 299–308 (2016).
5. M. H. Riaz et al., "The optimization of vertical bifacial photovoltaic farms for efficient agrivoltaic systems," *Sol. Energy* **230**, 1004–1012 (2021).
6. J. B. Jahangir et al., "A critical analysis of bifacial solar farm configurations: theory and experiments," *IEEE Access* **10**, 47726–47740 (2022).
7. O. A. Katsikogiannis, H. Ziar, and O. Isabella, "Integration of bifacial photovoltaics in agrivoltaic systems: a synergistic design approach," *Appl. Energy* **309**, 118475 (2022).
8. X. Sun et al., "Optimization and performance of bifacial solar modules: a global perspective," *Appl. Energy* **212**, 1601–1610 (2018).
9. G. M. Tina et al., "Assessment of the electrical and thermal performances of building integrated bifacial photovoltaic modules," *J. Clean. Prod.* **313**, 127906 (2021).
10. B. Soria et al., "A study of the annual performance of bifacial photovoltaic modules in the case of vertical facade integration," *Energy Sci. Eng.* **4**(1), 52–68 (2016).
11. S. Pal, "Tracing the light: designing reflectors for bifacial photovoltaic yield enhancement under outdoor irradiance," PhD Thesis, University of Twente (2022).
12. M. Alam, M. S. Gul, and T. Muneer, "Performance analysis and comparison between bifacial and monofacial solar photovoltaic at various ground albedo conditions," *Renew. Energy Focus* **44**, 295–316 (2023).
13. M. T. Patel et al., "Temperature-dependent energy gain of bifacial PV farms: a global perspective," *Appl. Energy* **276**, 115405 (2020).
14. M. P. Brennan et al., "Effects of spectral albedo on solar photovoltaic devices," *Sol. Energy Mater. Sol. Cells* **124**, 111–116 (2014).
15. T. C. R. Russell et al., "The influence of spectral albedo on bifacial solar cells: a theoretical and experimental study," *IEEE J. Photovolt.* **7**, 1611–1618 (2017).
16. H. Ziar et al., "A comprehensive albedo model for solar energy applications: geometric spectral albedo," *Appl. Energy* **255**, 113867 (2019).
17. J. Lehr et al., "Energy yield of bifacial textured perovskite/silicon tandem photovoltaic modules," *Sol. Energy Mater. Sol. Cells* **208**, 110367 (2020).
18. S. S. Pal et al., "Understanding and benchmarking ground reflectors for bifacial photovoltaic yield enhancement," *IEEE J. Photovoltaics* **14**, 160–169 (2024).

19. S. Bundo et al., "Spectro-angular analysis of roadside-integrated bifacial solar power systems with reflecting sound barriers," *JPhys Photonics* **6**, 025006 (2024).
20. B. Walter et al., "Microfacet models for refraction through rough surfaces," in *18th Rendering Tech.*, pp. 195–206 (2007).
21. W. Qin et al., "Characterizing leaf geometry for grass and crop canopies from hotspot observations: a simulation study," *Remote Sens. Environ.* **80**, 100–113 (2002).
22. J. T. Woolley, "Reflectance and transmittance of light by leaves," *Plant Physiol.* **47**, 656–662 (1971).
23. S. Jacquemoud et al., "Estimating leaf biochemistry using the PROSPECT leaf optical properties model," *Remote Sens. Environ.* **56**, 194–202 (1996).
24. M. A. Shah, J. Kontinnen, and S. Pattanaik, "Real-time rendering of realistic-looking grass," in *Proc. 3rd Int. Conf. Comput. Graph. Interact. Tech. Australasia and South East Asia, GRAPHITE*, Association for Computing Machinery, New York, NY, pp. 77–82 (2005).
25. S. Sandmeier et al., "Physical mechanisms in hyperspectral BRDF data of grass and watercress," *Remote Sens. Environ.* **66**, 222–233 (1998).
26. P. R. Forsström et al., "Multi-angular reflectance spectra of small single trees," *Remote Sens. Environ.* **255**, 112302 (2021).
27. A. Kuusk, "The hot spot effect in plant canopy reflectance," in *Photon-Vegetation Interactions: Applications in Optical Remote Sensing and Plant Ecology*, R. B. Myneni and J. Ross, Eds., pp. 139–159, Springer, Berlin, Heidelberg (1991).
28. D. L. B. Jupp and A. H. Strahler, "A hotspot model for leaf canopies," *Remote Sens. Environ.* **38**, 193–210 (1991).
29. L. M. Horst, "Modelling the spectro-angular reflectance of grass for accurate bifacial photovoltaic yield calculation," Master's Thesis, University of Twente (2023).
30. J. M. DeYoung, "Properties of tabulated bidirectional reflectance distribution function," PhD Thesis, University of British Columbia (1996).
31. A. M. Baldridge et al., "The ASTER spectral library version 2.0," *Remote Sens. Environ.* **113**, 711–715 (2009).
32. K. Boulanger, S. N. Pattanaik, and K. Bouatouch, "Rendering grass in real time with dynamic lighting," *IEEE Comput. Graph. Appl.* **29**, 32–41 (2009).
33. J. Silvertown et al., "Rainfall, biomass variation, and community composition in the park grass experiment," *Ecology* **75**(8), 2430–2437 (1994).
34. "Kunstgras naturel 2.0–natuurlijk kunstgras," https://www.kunstgrasnet.nl/naturel (accessed 2024-12-05).
35. A. Rikhof et al., "Optimizing bifacial PV performance: the impact of reflectors and free space luminescent solar concentrators on winter yield," *Sol. Energy Mater. Sol. Cells* **282**, 113323 (2025).
36. M. Barragán Sánchez-Lanuza et al., "Spectral irradiance, ground and crop dynamic reflectance: key determinants in predicting photocurrent for agrovoltaic systems," *Energy Convers. Manage.* **312**, 118572 (2024).

Jelle Westerhof is a graduate student in applied physics at the University of Twente, Netherlands. He completed the university's ATLAS honors program for his bachelor's and received a student fellowship during his master's for an internship at ICFO, Barcelona. His current research focuses on light–matter interactions for photovoltaics.

Leonie M. Horst received a master with distinction in sustainable energy technology from the University of Twente (NL) in 2023. During her thesis, she developed ray tracing software to simulate the reflectance of grass such to compute its contribution to the yield of a solar panel.

Anne Rikhof earned her master's degree in sustainable energy technology from the University of Twente (NL), specializing in simulation techniques for energy generation technologies. She is currently pursuing an engineering doctorate (EngD) focusing on the simulation of biomass combustion.

Shweta S. Pal completed her master's degree in physics from the Institute of Chemical Technology, Mumbai, India. She earned her PhD and pursued postdoctoral research at the University of Twente, focusing on optical optimizations for bifacial solar cells. Currently, she works as an optical engineer at ASML, Netherlands.

Dmitry Busko studied physics in Belarus. In 2003 he joined Stepanov Institute of Physics NASB as young researcher. Afterwards, he did a PhD in Max-Planck Institute of Polymer Research in Mainz (Germany). Since 2015, he is a postdoctoral researcher in IMT, Karlsruhe Institute of Technology (Germany). His research activities lie in development of characterization methods

of optically active materials with a main focus on up- and down-conversion materials for plastic recycling and solar energy applications.

Bryce S. Richards studied physics and electrical engineering in New Zealand and Australia. In 2006, he joined Heriot-Watt University (UK) as a lecturer, being promoted to full professor in 2008. Since 2014, he is professor of nanophotonics for energy in the Faculty of Electrical Engineering at the Karlsruhe Institute of Technology (Germany). His primary research areas lie in spectral conversion (up- and down-conversion), the application of luminescent materials for solving real-world problems, and solar-energy harvesting.

Rebecca Saive is a professor of applied physics at the University of Twente, Netherlands. Her research focuses on advanced light management techniques for photovoltaic systems. She earned her PhD from the University of Heidelberg, Germany, and completed postdoctoral research at the California Institute of Technology. She co-founded a startup in the semiconductor sector and was named one of the Innovators Under 35 Europe and Global by *MIT Technology Review*.